C. R. Palevol 16 (2017) 71–81

Contents lists available at ScienceDirect

Comptes Rendus Palevol

www.sciencedirect.com

Human palaeontology and prehistory

A human parietal fragment from the late Early Pleistocene Gran Dolina-TD6 cave site, Sierra de Atapuerca, Spain

Fragment de pariétal humain de la fin du Pléistocène inférieur du site de la grotte de Gran Dolina-TD6, Sierra de Atapuerca, Espagne

Emiliano Bruner[a], Hana Píšová[b,c], Laura Martín-Francés[a], María Martinón-Torres[d], Juan Luis Arsuaga[e,f], Eudald Carbonell[g,h], José María Bermúdez de Castro[a,d,*]

[a] *Grupo de Paleobiología, Centro Nacional de Investigación sobre la Evolución Humana, Burgos, Spain*
[b] *Katedra Antropologie a Genetiky Člověka, Univerzita Karlova, Prague, Czech Republic*
[c] *Antropologické Oddělení, Národní Muzeum, Prague, Czech Republic*
[d] *Department of Anthropology, University College of London, London, United Kingdom*
[e] *Área de Paleontología, Departamento de Geología, Universidad de Alcalá de Henares, 28871 Alcalá de Henares, Spain*
[f] *Centro Mixto UCM-ISCIII de Evolución y Comportamiento Humanos, Madrid, Spain*
[g] *Institut Català de paleoecologia Humana I Evolució Social (IPHES), Marcel.li Domingo s/n, 43007 Tarragona, Spain*
[h] *Laboratory of Human Evolution, Institute of Vertebrate Paleontology and Paleoanthropology (IVPP), Chines Academy of Sciences, 100044 Beijing, China*

ARTICLE INFO

Article history:
Received 30 November 2015
Accepted after revision 8 February 2016
Available online 26 April 2016

Handled by Roberto Macchiarelli

Keywords:
Late Early Pleistocene
Parietal bone
Cranial thickness
Craniovascular morphology

ABSTRACT

The TD6-2 level of the Gran Dolina cave site (Sierra de Atapuerca, Burgos, Spain) has yielded an assemblage of about 170 human fossil remains dated to > 800 ka (probably MIS 21) and assigned to the species *Homo antecessor*. In this study, we describe for the first time a large portion of a parietal bone (ATD6-100/168). The morphology of the fractures on the bones is compatible with a peri-mortem trauma. The superior parietal areas are flat. There is a large parietal foramen and one smaller accessory parietal foramen. Middle meningeal vessels are not particularly developed, but they are distributed in both anterior and posterior districts, with the parietal vasculature originating from the posterior branch. The meningeal vessels show multiple minor connections with the pericranial and diploic vascular systems. The diploe is not particularly developed, and large diploic channels are not detected. The bone is thin when compared with adult fossil humans, and equivalent to juvenile values. All these characters suggest that the parietal ATD6-100/168 probably belonged to a juvenile individual, with plesiomorphic endocranial traits similar to those described for *H. ergaster/erectus*. The derived temporal, maxillary and dental traits in *Homo* antecessor and the primitive parietal morphology further point to distinct (mosaic) patterns of morphological evolution of face and braincase.

Mots clés :
Fin du Pléistocène inférieur
Os pariétal

RÉSUMÉ

Le niveau TD6-2 de la grotte de Grand Dolina (Sierra de Atapuerca, Burgos, Espagne) a fourni un assemblage d'environ 170 restes humains d'âge > 800 ka (probablement MIS 21) et assignés à l'espèce *Homo antecessor*. Dans cette étude, nous décrivons pour la première

* Corresponding author at: Centro Nacional de Investigación sobre la Evolución Humana, Paseo Sierra de Atapuerca 3, 09002 Burgos, Spain.
E-mail address: josemaria.bermudezdecastro@cenieh.es (J.M. Bermúdez de Castro).

http://dx.doi.org/10.1016/j.crpv.2016.02.002
1631-0683/

Épaisseur crânienne
Morphologie cranio-vasculaire

fois une large portion d'une voûte pariétale (ATD6-100/168). La morphologie des fractures sur les os est compatible avec un trauma peri-mortem. Les zones pariétales supérieures sont plates. Il y a un grand foramen pariétal et un foramen pariétal accessoire plus petit. Les vaisseaux méningés centraux ne sont pas particulièrement développés, mais ils sont répartis à la fois entre les secteurs antérieur et postérieur, avec une vascularisation pariétale provenant de la branche postérieure. Les vaisseaux méningés montrent de multiples connexions mineures avec les systèmes péricrânial et diploïque. Le diploe n'est pas particulièrement développé et de grands canaux diploïques ne sont pas détectés. L'os est mince en comparaison de celui des humains fossiles adultes et équivalent à celui des juvéniles. Tous ces caractères suggèrent que le pariétal ATD6-100/168 appartient probablement à un individu juvénile, avec des traits endocrâniens plésiomorphes, analogues à ceux décrits pour *H. ergaster/erectus*. Notre étude souligne le patron en mosaïque de l'évolution morphologique.

1. Introduction

The Sierra de Atapuerca is located 14 km east of the city of Burgos (northern Spain), with an area of about 25 km^2 and a maximum altitude of 1082 m above sea level. In the last 40 years, the karst of this area has provided several archaeological and paleontological sites, including those discovered after the section of a railway opened at the end of the 19th century (Trinchera del Ferrocarril). One of these infillings is named Gran Dolina (TD), and contains a large Pleistocene sedimentary sequence about 27 m deep and a maximum width of 17 m. In 1987, Gil et al. (1987) divided the Gran Dolina section from bottom to top into 11 levels: TD1 to TD11. About 170 human fossil remains were recovered from the TD6 level during the 1994–1996 and 2003–2004 field seasons (e.g. Bermúdez de Castro et al., 1999; Carbonell et al., 1995). The study of the cranial and dental remains evinced a unique combination of primitive and derived cranial and dental features regarding the *Homo* clade and we proposed a new species, *Homo antecessor* (Bermúdez de Castro et al., 1997; see also Bermúdez de Castro et al., 2015a, 2015b). The bones are fragmentary and the accumulation was explained as the result of one or more events of cannibalism (Carbonell et al., 2010; Fernández-Jalvo et al., 1999).

Currently, there is a vertical cut of the Gran Dolina section in progress. This work has allowed a stratigraphic refinement of the TD6 section (Fig. 1), as well as of other Gran Dolina levels (e.g., Bermúdez de Castro et al., 2008; Campaña et al., 2015). For instance, the TD6 level has been divided in three sublevels: TD6-1, TD6-2, and TD6-3. The human fossils, as well as more than 300 artefacts and several thousands of micro- and macromammal fossil remains (Carbonell et al., 1999; Cuenca-Bescós et al., 1999; García and Arsuaga, 1999; van der Made, 1999) come from the sublevel TD6-2 level. Parés and Pérez-González (1995, 1999) observed a polarity reversal between TD7 and TD8, interpreted as the Matuyama/Brunhes boundary, meaning that levels TD8-TD11 were deposited during the Middle Pleistocene, whereas levels TD7-TD1 were attributed to the Early Pleistocene. The combination of paleomagnetic data and US-ESR ages suggests an age range between 780 and 866 ka for the so-called Aurora Stratum (Falguères et al., 1999). Thermoluminiscence (TL) dates on samples taken at the TD7 level, one meter below the Brunhes/Matuyama boundary give a weighted mean age of 960 ± 120 ka for TD7 (Berger et al., 2008). The ESR dating applied to optically bleached quartz grains gives dates between 601 ± 88 ka and 947 ± 90 ka (Moreno et al., 2015). These authors also obtained dates of 734 ± 128 ka and 852 ± 144 ka for the TD7 level, from samples taken under the Matuyama/Brunhes boundary. Using thermally transferred OSL (TT-OSL) dating of individual quartz grains, Arnold et al. (2014) obtained a weighted mean age of 846 ± 57 ka for the TD6 level. Finally, Arnold and Demuro (2015) have undertaken a series of TT-OSL suitability assessments on known-age samples from TD6. Using this method, they obtained a weighted average age of 851 ± 46 ka for TD6-3. Summarizing, and considering the biostratigraphic information from TD6 (Cuenca-Bescós et al., 1999, 2015), we consider that the TD6 hominins could be assigned to the MIS 21.

During the 2003 field season, three fragments of a right parietal bone were found at the TD6 level (Fig. 2). The anterior fragment is labelled as ATD6-100, whereas the two posterior fragments are labelled as ATD6-168. The parietal ATD6-100 + ATD6-168 (ATD6-100/168) was recovered from the sublevel named "Jordi", which is at the bottom of the so-called "Aurora archaeostratigraphic set, AAS" (Bermúdez de Castro et al., 2008). The AAS correlates with the Aurora Stratum defined in 1995 (Carbonell et al., 1995, and see also a lithostratigraphic description in Parés and Pérez-González, 1999). The Aurora Stratum represents a condensed deposit of the six well-differentiated layers of the AAS (Bermúdez de Castro et al., 2008). Therefore, it is very difficult to know the precise relationship between ATD6-100/168 and the human fossils recovered during the excavation of the Aurora Stratum in 1994–1995. The well-preserved hemimandible ATD6-96 (e.g. Bermúdez de Castro et al., 2015a, 2015b; Carbonell et al., 2005) was also recovered in Jordi, few centimeters away from ATD6-100/168.

The aim of this report is to describe this parietal fragment and to provide metric and morphological features of its external and internal surfaces.

2. Methods

The parietal bone was analyzed with a microtomographic Scanco Medical μCT80 scanner with an isometric

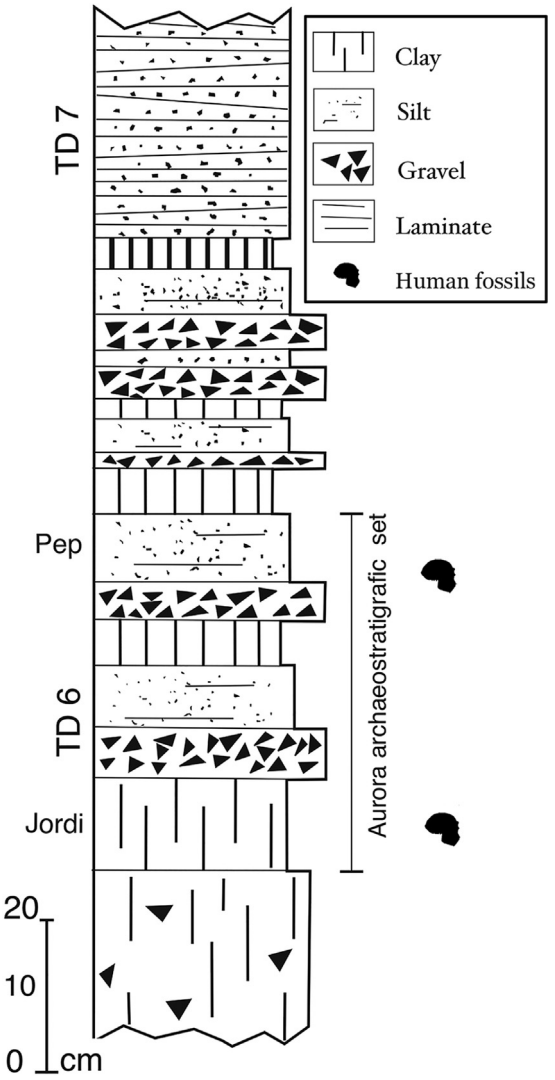

Fig. 1. Upper sequence of the lithostratigraphic unit TD6 from the Gran Dolina cave infilling (Matuyama Chron), which includes the "Aurora archaeostratigraphic set" (AAS), also known as TD6-2. All the human fossils of the *Homo antecessor* hypodigm have been recovered from this section of the unit TD6.

Fig. 1. Séquence supérieure de l'unité stratigraphique TD6 du remplissage de la grotte de Gran Dolina (Matuyama Chron), qui inclut l'« ensemble archéostratigraphique Aurora » (AAS), aussi connu sous la dénomination TD6-2.

Modified from Bermúdez de Castro et al., 2008.

voxel of 37 μm (slice thickness 37 μm, slice increment 37 μm; pixel resolution 37 μm), and a matrix of 2048 × 2048 pixels. For macroanatomic observations, data were reduced and reformatted to a 1024 × 1024 pixel matrix, with an isometric voxel of 74 μm. Tomographic data were visualized and segmented with MIMICS 18.0 (Materialise) and ImageJ 1.48q (Schneider et al., 2012). Ten chords were used to compare the physical specimen and the digital replica, giving an average discrepancy of 0.5 mm (range 0.0–0.8 mm), mostly due to uncertainty associated with the localization of reference landmarks. This discrepancy involves an error of 0.3%–2.3%. Measures of cortical thickness give an average discrepancy of 0.3 mm (8%). Thickness was measured at 10 points distributed along the perimeter of the fragment, as to give a general overview of the thickness variation: six points lateral to the sagittal suture, and four points at the lower boundary of the parietal fragment, in areas without major bone damages. These values were compared with the metrics reported in Lieberman (1996) for the parietal eminence in fossil hominids (after Nawrocki, 1991 and Minugh-Purvis, 1988) and for the vertex in recent European and Australian Aborigines (after Brown et al., 1979; Roche, 1953). Microscopic inspection of the parietal fragment, including stereomicroscope and μCT imaging, was performed to investigate and describe the fractures affecting the bone and to determine the timing (ante-, peri- or postmortem) of the fracture events.

3. Description of the ATD6-100/168 parietal bone

ATD6-100 represents the anterior portion of the parietal bone, missing all the areas of the sutures. ATD6-168 includes the sagittal and posterior areas (including the sagittal and lambdoid sutures) and the upper part of the parietal squama until the parietal boss, whose tip is missing. Fig. 3 shows the digital replica of the fossil, and a drawing presenting specific features. Fig. 4 shows tomographic sections and a 3D transparency rendering. The sagittal and lambdoidal sutures are largely preserved, with chords of 75 and 48 mm, respectively. The lambda is preserved. Bregma was probably few centimeters forward to the anterior edge of the suture, and this suggests that possibly the anterior border of the fragment was not far from the coronal suture. The asterionic area is not preserved.

The parietal presents several fractures at different locations. Two major fractures affect its anterior and lateral aspects where the sagittal and temporal sutures are incomplete or missing. Moreover, the parietal eminence presents an angular fracture that has affected its tip. The morphology of the two large fractures are characterized by straight edges where the diploe, inner and outer tables do not exhibit further involvement, and their morphologies are clearly differentiated. The edges of these fractures are whitish, whereas the rest of the bone is more brownish (sediment) in colour. In contrast, the fracture affecting the parietal boss presents ragged and oblique edges. In this case, the outer and inner tables form a beveled cut where the inner table is missing a portion (flake of bone). There are two horizontal lines irradiating from this fracture following a medial/sagittal direction and, finally, there is no color difference between the margins of the fracture and the rest of the bone.

The parietal eminence is marked and strongly bossed. The marked bossing at the lower parietal area and the flat superior surface suggest that the specimen could have displayed the classical archaic human "tent-like" posterior profile. Such interpretation is however affected by the uncertainty associated with the limited anatomical information available. The bone presents a large parietal foramen, positioned at 8 mm from the sagittal suture, and 33 mm from the lambdoidal suture. Ectocranially, there are traces of a vessel running orthogonally from the foramina to the sagittal suture. The parietal foramen has an approx-

Fig. 2. The right parietal ATD6-100/168 from the site of the Gran Dolina, in ventral (endocranial) and dorsal (ectocranial) views.
Fig. 2. Pariétal droit ATD6-100/168 du site de Gran Dolina, en vues ventrale (endocrânienne) et dorsale (ectocrânienne).

imate length of 7.5 mm, with external diameters around 2.1 mm and minimum internal lumen of 0.7 mm. It is surrounded by a thick ring of dense bone, isolating the channel from the surrounding diploe.

The endocranial surface shows many vascular traces. Two large anterior branches can be interpreted as being part of the anterior network of the middle meningeal artery. Two large posterior branches can be interpreted as the middle (obelic) ramus of the middle meningeal artery. The largest one runs until the parietal foramen and enters the channel. Possible traces of the posterior (lambdatic) branch are limited to a single thin imprint running parallel to the lambdoidal suture. Although the middle branches originate from the posterior regions, the anterior branches are also large and wide, associated with minor local vascular networks. Traces of several minor vessels can be seen parallel to the main imprints. The branch entering the parietal foramen shows also two minor vessels reaching the area of the superior sagittal sinus. There are many minor vascular entries on the endocranial surface. These channels can be recognized after visual inspection, and the tomographic analysis shows that they enter the diploe without crossing the outer table. Many of these minor vascular accesses lie along the traces of the middle meningeal vessels. Most of these minor passages are mostly concentrated towards the lambda. A second smaller parietal foramen (accessory parietal foramen) is detected in the middle of this posterior spotted area, close to the lambda. The depression of the superior sagittal sinus alongside the sagittal suture is visible and large. At least two large venous lacunae can be recognized lateral to the central and anterior portion of the superior sagittal sinus. Both lacunae are positioned at the end of the most central vessels of the anterior and middle branches of the middle meningeal network. A third lacuna is likely present in the posterior region, between the lambdatic and obelic branches of the meningeal artery. There are no visible arachnoid granulations.

The inner table, the outer table, and the diploe, are clearly visible in the tomographic sections. The average thickness of the parietal, measured at 10 different positions, is 4.4 ± 0.9 mm. If we measure it at 10 positions in areas with a diploic layer, the average thickness is 5.3 mm. When present, the diploe occupies on average $40\% \pm 6\%$ of the bone thickness. The diploe is more developed close to the sutures and throughout the squama, being almost absent in the anterior and lower portions of the bone. There are no visible diploic channels, and therefore the diploic vasculature is supposed to be limited to the intertrabecular space or associated with minor passages. The thicker area is along the posterior tract of the sagittal suture. The thinner areas can be found approaching the temporal and frontal borders. The bad preservation of the inner table in the anterior areas can produce a minor bias in their thickness value. The outer table is generally denser than the inner table.

On Fig. 5, the values from ATD6-100/168 are compared with the data presented in Lieberman (1996). Thickness in ATD6-100/168 is reduced, and closer to the low values of modern humans more than to any fossil group. If we consider the ontogenetic variation, the figure in ATD6-100/168 is comparable with an age > 5.5 yr for modern humans and > 2.5 yr for Neandertals. On average, the value may be compatible with an age between 5 and 12 yrs. When using values from modern humans alone, the figure measured in ATD6-100/168 is comparable with an age between 5 and 16 years, and an average value of around 8–10 years of age.

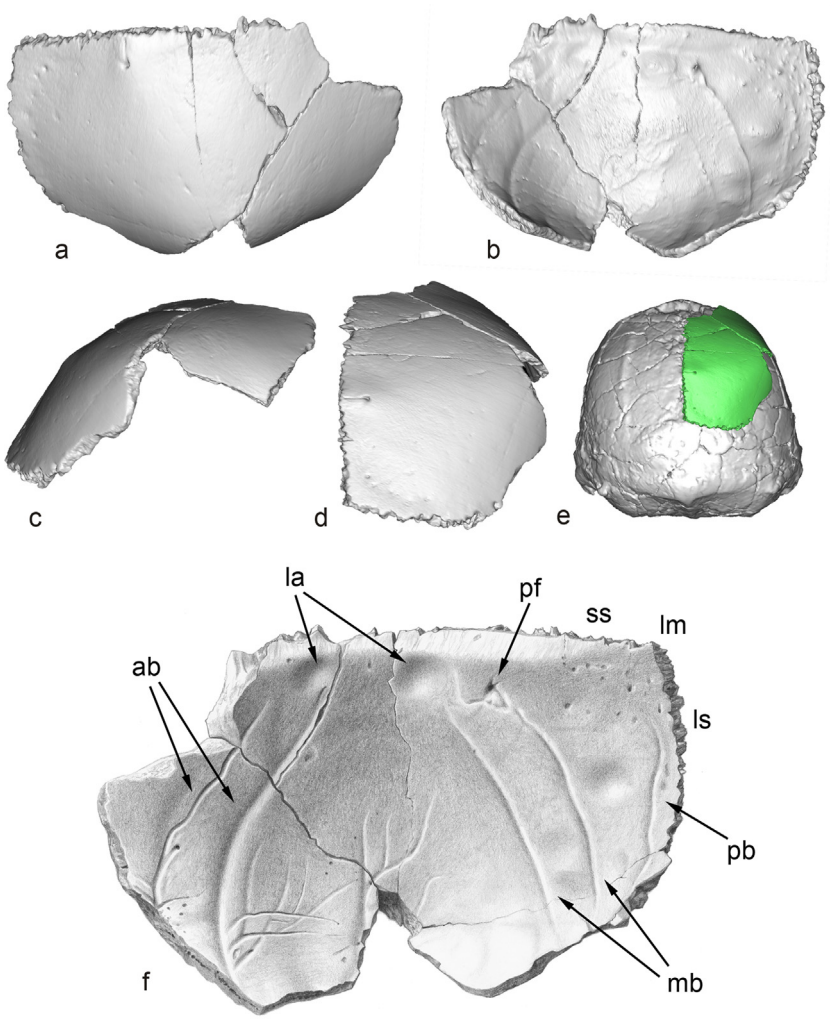

Fig. 3. Digital replica of the parietal ATD6-100/168 in dorsal (a), ventral (b), lateral (c) and posterior (d) views. The parietal (green) is superimposed on the digital replica of KNM-ER3733 in posterior view (e). The drawing of the parietal bone (f) shows the details of the vascular traces: ab: anterior branches of the middle meningeal vessels; la: lacunae; lm: lambda; ls: lambdoid suture; mb: middle branches of the middle meningeal vessels; pb: posterior branch of the middle meningeal vessels; pf: parietal foramen; ss: sagittal suture.
Fig. 3. Réplique digitale du pariétal ATD6-100/168 en vues dorsale (a), ventral (b), latérale (c) et postérieure (d). Le pariétal (en vert) est superposé sur la réplique digitale de KNM-ER3733 en vue postérieure (e). Le dessin de l'os pariétal (f) montre les détails des traces des vaisseaux : ab : branches antérieures des vaisseaux méningés centraux ; la : lacune ; lm : lambda ; ls : suture lamdoïde ; mb : branches centrales des vaisseaux méningés centraux ; pb : branche postérieure des vaisseaux méningés centraux ; pf : foramen pariétal ; ss : suture sagittale.

4. Discussion

4.1. Bioarchaeology and taphonomy

Given its chrono-stratigraphic context, is highly likely that the parietal ATD6-100/168 belongs to *H. antecessor*, a taxon that was described on the basis of a large set of facial, dental, cranial and postcranial elements (Bermúdez de Castro et al., 1997). Regarding the cranial vault, the temporal squama of *H. antecessor* was described as high and convex, a synapomorphy shared with *H. sapiens* and *H. neanderthalensis* (Arsuaga et al., 1999; Bermúdez de Castro et al., 1997). However, the morphology of the parietal was not known. Taking into account the absence of comparable specimens with similar geochronological position, this specimen is currently the only consistent evidence we have on the parietal bone of the species living in Europe during Lower Pleistocene.

The fragment suggests small cranial dimensions, and it can be interpreted as belonging to a juvenile, as it happens with other human remains from the same site (Bermúdez de Castro et al., 2015a). Unfortunately, it is not possible to connect physically ATD6-100/168 with other cranial remains from subadult individuals recovered from TD6-2 (see Arsuaga et al., 1999). The frontal squama ATD6-15 (subadult) could belong to the same individual. However, the absence of physical connection between the two fossils hampers the confirmation of this hypothesis. The bone shows several fractures, which can provide information on the individual history of the specimen. Fracture is a type

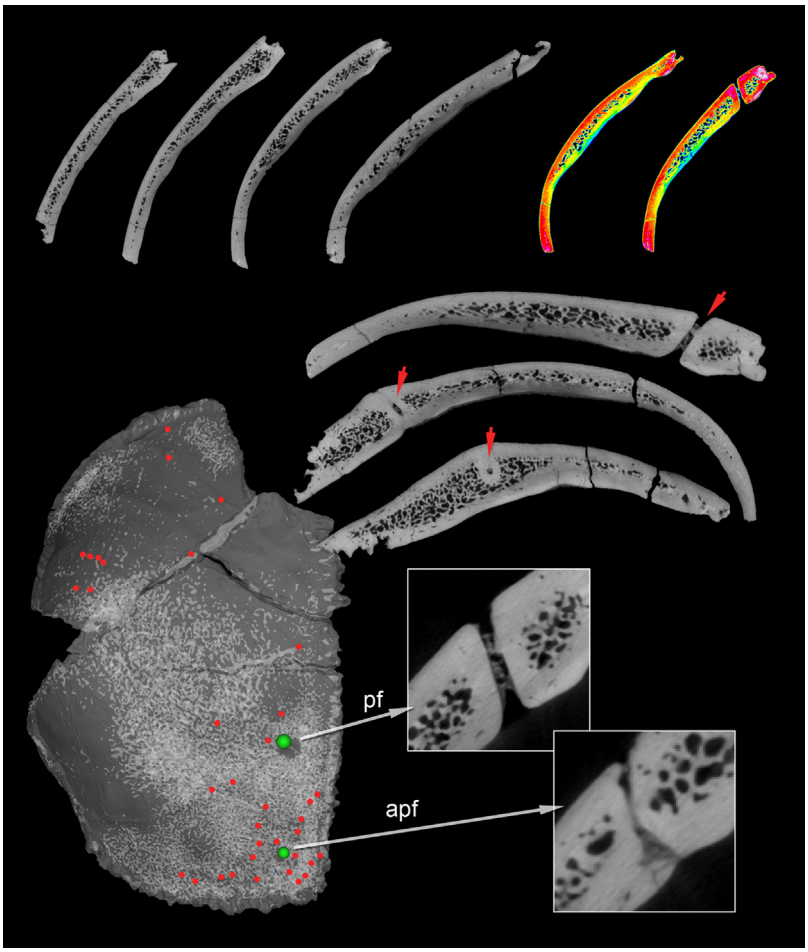

Fig. 4. Tomographic sections and rendering of the parietal ATD6-100/168. On the upper row, a set of slices shows the bone thickness and distribution of the diploe. Colored maps show the distribution of the density values (red: high density; blue: low density). In the middle row, three slices show the passage of the parietal foramen (red arrows) in sagittal, coronal, and transversal sections. A thick ring of dense bone separates the parietal foramen. In the lower area, a transparent rendering of the bone shows the distribution of the diploe (whiter areas), the position of the minor vascular channels (red points), and the position of the parietal foramina (green points; pf: parietal foramen; apf: accessory parietal foramen). The two canals can be seen in the zoomed images.
Fig. 4. Sections tomographiques et interprétation du pariétal ATD6-100/168. Sur le rang supérieur, une série de lames montre l'épaisseur de l'os et la distribution de la diploé. Les cartes en couleur indiquent la répartition des valeurs de densité (rouge : forte densité ; bleu : faible densité). Dans le rang intermédiaire, trois lames minces montrent le passage du foramen pariétal (flèches rouges) en sections sagittale, coronale et transversale. Un anneau épais d'os dense cloisonne le foramen pariétal. Dans la zone inférieure, une vue transparente de l'os montre la distribution de la diploé (zones plus blanches), la position de canaux vasculaires mineurs (points rouges) et celle des foramens pariétaux (points verts ; pf : foramen pariétal ; apf : foramen pariétal accessoire). Les deux canaux peuvent être observés en images « zoom ».

of trauma and consists of the disruption of the bone structure, normally involving the adjacent soft tissues (Bennike, 2008; Ortner, 2003). The determination of the timing of the injury is crucial to suggest a possible cause of death. In general, signs of bone healing are indicative of a pre-mortem event. However, the distinction between peri- from post-mortem fractures is a more complex task (Boylston, 2000; Bennike, 2008; Buikstra and Uberlaker, 1994; Sauer, 1998). The pattern of fracture is the main criteria to determine the timing of the event. Fresh bone is more liable and tends to fracture in irregular edges. On the contrary, dry bone is more brittle, due to the lack of collagen, grease and fluid, and fractures in more regular fragments. Another criterion is the coloration of the edges. Changes in coloration would indicate a postmortem event, whether same coloration could indicate that the lesion occurred around the time of bone deposition (Bennike, 2008; Sauer, 1998; Waldron, 2009). The edges of the fracture affecting the parietal boss present the same brownish (sediment) coloration that the rest of the bone. This contrasts with the described whitish edges exhibited by the fracture that affect the tip of the parietal eminence. Fractures have being classified depending on the type of force exerted on the bone (Ortner, 2003) or its morphology (Waldron, 2009). Love et al. (2011) classified the fractures of the skull based on their morphology as linear, depressed, diastatic, basilar and crushing. Within these the most frequent types are linear (non-displaced fractures that cross part or the whole skull resulting from low energy blunt force to a wide area of the skull), followed by depressed. The latter results from high-energy forces, and the range of severity determines their morphology: from depression to inward fractures with displaced

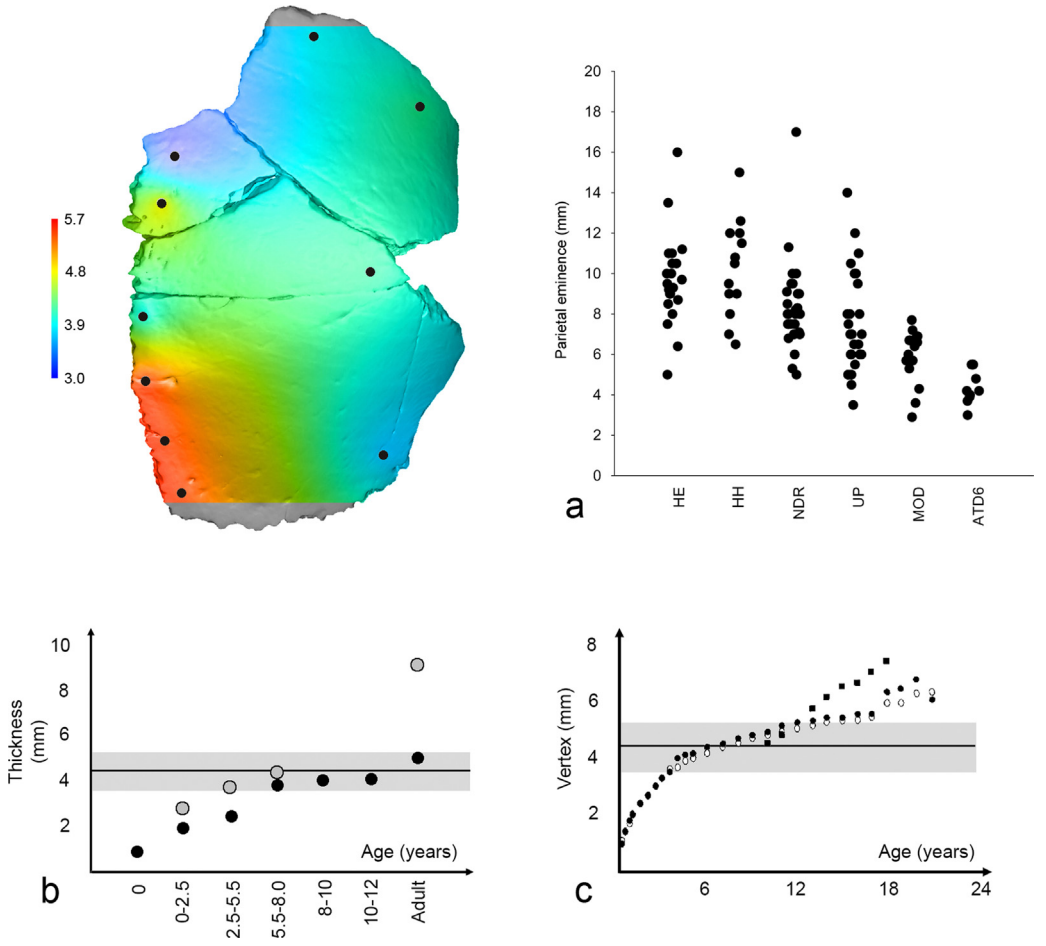

Fig. 5. Thickness was measured at 10 points (black dots). A color map was computed interpolating the values through a quadratic function with PAST 2.17c (Hammer et al., 2001) for visualization purpose (red: thicker; blue: thinner; scale in mm). The plots show the values for ATD6-100/168 compared with the data from Lieberman, 1996: a: parietal eminence thickness for main human taxa (HE: *Homo erectus*; HH: *Homo heildelbergensis*; NDR: Neandertals; UP: *Homo sapiens*, Upper Paleolithic; MOD: living humans) and ten values from ATD6; b: age groups and parietal eminence thickness (black dots: modern humans; grey dots: Neandertals) showed with the ATD6-100/168 mean value (line) and standard deviation (shaded area); c: age and vertex thickness (black dots: recent European males; white dots: recent European females; black squares: Australian aborigines) showed with the ATD6-100/168 mean value (line) and standard deviation (shaded area).

Fig. 5. L'épaisseur a été mesurée en 10 endroits (taches noires). Une carte en couleur a été bâtie par ordinateur en interpolant les valeurs par une fonction quadratique avec PAST 2.17c (Hammer et al., 2001) dans un but de visualisation (rouge : le plus épais ; bleu : le plus mince ; échelle en millimètres). Les repères montrent les valeurs pour ATD6-1200/168, comparées aux données de Lieberman, 1996 : a : épaisseur de l'éminence pariétale pour les principaux taxons humains (HE : *Homo erectus* ; HH : *Homo heidelbergensis* ; NDR : Néandertals ; UP : *Homo sapiens*, Paléolithique supérieur ; MOD : Hommes vivants) et 10 valeurs de l'ATD6 ; b : groupes d'âge et épaisseur de l'éminence pariétale (points noirs : hommes modernes ; points gris : Néandertals) présentés avec la valeur moyenne (ligne) pour ATD6-100/168 et la déviation standard (zone ombrée) ; c : âge et épaisseur du vertex (points noirs : mâles européens récents ; points blancs : femelles européennes récentes ; carrés noirs : aborigènes australiens) présentés avec la valeur moyenne (ligne) et la déviation standard (zone ombrée) pour ATD6-100/168.

fragments. The parietal is the common location for this type of fractures.

Considering the signs recorded (ragged and beveled edges, the most-likely inward displacement/loss of the inner table, location, radiating lines and coloration) in ATD6-100 and ATD6-168, the lesion could correspond to a depressed fracture resulting from a high-energy force to the parietal bone. According to Love et al. (2011) in violent deaths the cranial bone most frequently involved is the parietal, followed by the occipital, frontal and temporal. The signs are also consistent with fresh bone fracture and suggest that it occurred around the time of the individual's' death. A cannibalistic activity was hypothesized to be associated with the fossil collection recovered in Gran Dolina (Carbonell et al., 2010; Fernández-Jalvo et al., 1999; Saladié et al., 2012), in agreement with the peri-mortem time of the event. In the context of a cannibal event, a violent trauma would be highly possible, but the evidence is too fragmentary to make a diagnosis. Evidences of cranial fracture and trauma in the fossil record are numerous (e.g., Brain, 1993; Wu et al., 2011). However, only in a very few cases it was possible to unequivocally associated the trauma with the cause of death (see Cranium 17 from Sima de los Huesos; Sala et al., 2015). Future discoveries may help to clarify the nature of the fracture in the *H. antecessor* parietal.

4.2. Paleoneurology and craniovascular traits

From an evolutionary point of view, the parietal bone is relevant because it underwent different changes within the radiation of the human genus (Bruner et al., 2015; Holloway, 1981). Pleistocene specimens assigned to *Homo ergaster* and *H. erectus s.s.* display a shared plesiomorphic parietal morphology, characterized by a parasagittal flattening of the upper surfaces (Bruner et al., 2015). In contrast, Neandertals show a lateral bulging of these areas, and modern humans expand further the superior parietal lobules through a notable longitudinal enlargement (Bruner, 2004; Bruner et al., 2003, 2011a). This parietal growth, specific of *H. sapiens*, is associated with an early postnatal stage only present in our species, and not in Neandertals or living apes (Gunz et al., 2010; Neubauer et al., 2009, 2010; Scott et al., 2014). Therefore, after the first year of age the parietal morphology can reveal its general species-specific final shape. Although incomplete, the parietal bone from ATD6-100/168 suggests an archaic phenoptype: the marked bossing is associated with the inferior parietal lobule (namely the supramarginal gyrus) and the superior parietal areas are flat and depressed. This parietal morphology is generally associated with human species such as *H. ergaster* and *H. erectus* (Bruner et al., 2003, 2015; Grimaud-Hervé, 1997).

The parietal foramina of ATD6-100/168 are interesting because the information available on these features is scarce, and any additional record adds to the development of a more extended database. Nonetheless, the feature per se cannot add much to the analysis of single specimens. ATD6-100/168 shows a large parietal foramen and a smaller accessory one approaching the lambda. Multiple parietal foramina with variable position and number, and presence of intracranial and extracranial accessory canals of inconstant diameter communicating with the diploe have been previously described in modern humans (Boryslawski et al., 2002; García Gil et al., 2015; Panteado and Santo Neto, 1985; Schelling, 1978; Stallworthy, 1932; Zenker and Kubik, 1996). However, multiple parietal foramina are rare, having a prevalence of 2.5% in modern populations (Boyd, 1930). Lang and Brückner (1981) mentioned that parietal foramen develops during the first year of life and its dimensions remain constant (in Braga and Boesch, 1997). Therefore, we must assume that the foramen in ATD6-100/168 has reached its final size. Parietal emissary foramina generally contain a common emissary vein connecting the intra and extracranial venous space (Boyd, 1930), and may supply anastomoses between the middle meningeal artery and the occipital artery, or with other pericranial vessels (Alvernie et al., 2006; Knott, 1881; Schelling, 1978; Yoshioka et al., 2006). Endocranially, the connections of anastomosing arteries are often clearly visible on the grooves of middle meningeal pathways leading towards the parietal foramina (Stallworthy, 1932). In ATD6-100/168, there is an ectocranial trace of a vessel from the foramen to the sagittal suture, although the pathways of the scalp arteries (occipital or pericranial) towards the parietal foramen are generally not visible (Yoshioka et al., 2006). At present, there is no information on the possible functional or structural meaning of these passages, and of their variations. The concentration of minor vascular passages around the lambda between the endocranial surface and the diploe is also a character common in humans, although quantitative data are lacking. The absence of arachnoid granulations may remark the young age of the subject, although also in this case data on these traits, supposed to be associated with aging, are incomplete (Grossman and Potts, 1974; Le Gros Clark, 1920).

The traces of the middle meningeal artery are frequently analyzed in paleoneurology, because of their variations among hominids (Bruner and Sherkat, 2008). Modern humans display a complex vascular network, mostly at the parietal surface, while non-modern species show simpler vascular systems (Bruner et al., 2005; Grimaud-Hervé, 1997). During morphogenesis, the complexity of these networks increases, mostly before 2 years of age (Saban, 1995). Although also in this case the exact functions of these vessels are not known, they may be involved in endocranial thermoregulation (Bruner et al., 2011b; Rangel de Lázaro et al., 2015). Archaic human species tends to have larger posterior branches, while modern humans and Neandertals display larger anterior vasculature (Grimaud-Hervé, 1997). In ATD6-100/168 the middle (obelic) branches probably originate from the posterior network, so it would fit the archaic pattern. Such scheme is named Adachi II pattern, a terminology based on the reciprocal relationships among the arterial branches (Falk, 1993; Falk and Nicholls, 1992). There is no evidence of a clear association between this vascular pattern and cranial morphology (Bruner et al., 2009), although its high frequency in Asian *H. erectus* suggests that it can be associated with braincases characterized by relatively large posterior districts, namely with large and projecting occipital areas and flat and small parietal areas (Bruner, 2015). Nonetheless, although in this case the parietal vasculature has a posterior origin, also the anterior branches show large traces and ramifications, and the overall vascular system looks equally distributed between the anterior and posterior districts.

4.3. Parietal thickness

Cranial thickness is another feature largely investigated in paleoanthropology, because of its variations among hominids (e.g., Balzeau, 2013; Curnoe, 2009; Gauld, 1996; Kennedy, 1991; Marsh, 2013; Nawrocki, 1991). Cranial thickness shows a positive allometry and marked correlation with body size in primates, with modern humans showing thicker frontal and parietal bones, and thinner temporal bones (Gauld, 1996). Although there are differences associated with sex and race, the large individual variation, the subtle differences, and the environmental influences, hamper a clear understanding of the role of these factors (e.g., Adeloye et al., 1975; Hwang et al., 2000; Jung et al., 2003; Lynnerup, 2001; Peterson and Dechow, 2002; Torres-Lagares et al., 2010). After a longstanding debate contrasting genetic and mechanical hypothesis, today is generally accepted that bone thickness is largely influenced by hormones and physiological responses, including physical activity and life-style with their consequent release of systemic factors (Anzelmo et al., 2014; Baab et al., 2010; Lieberman, 1996; Menegaz et al., 2010).

Most of the bone thickness growth occurs rapidly before the 6 years of age, with a following gradual increase until the age of 20 (Anzelmo et al., 2014; Hatipoglu et al., 2008; Li et al., 2011; Tsutsumi et al., 2013). The thickness of ATD6-100/168 is at the lower range of the modern humans' adult variation, but it is below the adult range in fossil species. According to the Neandertal age curve, its thickness is compatible with that of a juvenile specimen. Although all fossil hominids show thicker vault elements, a thin bone thickness can be also observed in the Mojokerto individual, an Asian specimen dated approximately to a period between 0.8 and 1.8 Ma and with an age between 1 and 8 years old (Balzeau et al., 2005). Following these general figures, the age of ATD6-100/168 can be tentatively bracketed between 4–12 years. Nonetheless, taking into account the limited information on thickness variations and the limited fossil record such estimation is largely speculative.

A special mention must be done for the diploic thickness. Actually, thick vault bones in archaic humans were largely due to the diploic layers (Copes and Kimbel, 2016). Although its value can be sensitive to special physiological and pathological conditions, preliminary analyses suggest age-dependent patterns (García Gil et al., 2015). According to these results, young ages are associated with a vascularized diploe, and adolescent bones are characterized by a reduction of the diploic space, which further increases in terms of thickness and vascularization in later adult age. However, in adults there is no apparently correlation between parietal thickness and vascularization (Eisová et al., 2016). Diploic vessels are also supposed to be relevant for thermoregulation, and their channels are probably more developed in modern humans than in extinct human species or in non-human primates (Hershkovitz et al., 1999; Rangel de Lázaro et al., 2015). In the case of ATD6-100/168, the diploic space occupies a percentage of the thickness (40%) comparable with low modern adult values (39–52%; Eisová et al., 2016), and no large diploic channels can be evidenced. Both features are in agreement with a young age. In the case of Mojokerto, the extension of the diploe was compared with a modern pattern with more than 3 years of age (Balzeau et al., 2005).

5. Conclusions

The ATD6-100/168 human remain from the site of the Gran Dolina, Atapuerca, represents the first parietal bone described for the *H. antecessor* species. According to the fractures on the bone, a peri-mortem trauma cannot be discarded. The vascular network is simple, with developed posterior meningeal branches. There is a large parietal foramen, and a secondary accessory one. The diploe is not much developed, and does not present large venous channels. According to the information available for modern and fossil human groups, the bone thickness of ATD6-100/168 is compatible with an age between 4 and 12 years. However, because of the large variation and limited knowledge on these characters, this result is largely tentative. The main changes of the parietal geometry occur in the first year of life (Gunz et al., 2010), and therefore its morphology is supposed to display the adult (mature) shape. The general appearance of the bone suggests a plesiomorphic phenotype. This species was hypothesized to show modern apomorphic traits in the facial skeleton and the temporal bone (Arsuaga et al., 1999; Bermúdez de Castro et al., 1997). The coexistence of facial and temporal derived features with more primitive traits in the parietal vault reveals a mosaic pattern of human evolution, that is particularly evident during Middle Pleistocene (e.g., Rightmire, 2008; Stringer, 2012). A similar evolutionary dissociation among some aspects of the face and the braincase was described for Middle Pleistocene specimens in Europe (Arsuaga et al., 2014), Asia (Wu and Bruner, 2016) and Africa (Bruner and Pearson, 2013). Such complex demographic and anatomical dynamics suggest caution when dealing with the interpretation of isolated or fragmented fossil remains.

Acknowledgements

The authors acknowledge all members of the Atapuerca Research Team for their dedication and effort. To Lucía López-Polin, from the IPHES Restoration and Conservation Department, for the cleaning of the specimen, and to Pilar Fernández Colón and Elena Lacasa Marquina, from the CENIEH Conservation and Restoration Department, for their work with the conservation and manipulation of the specimen. We also acknowledge The Leakey Foundation through the personal support of Gordon Getty and Dub Crook to one of the authors (MM-T). The drawing of the specimen on Fig. 3 is by Eduardo Saiz. Microtomography was performed at the Centro Nacional de Investigación sobre la Evolución Humana, Burgos. EB and HP are supported by the project "Cranial anatomy, anthropology, and vascular system", which is funded by the International Collaborative Research Grant (ICRG) of the Wenner-Gren Foundation. HP is also supported by Ministry of Culture of the Czech Republic (DKRVO 2016/19, National Museum, 00023272). EB is also supported by the Italian Institute of Anthropology. LMF is beneficiary of a Fundación Atapuerca Post-Doctoral Research Grant. This report has been supported by the Dirección General de Investigación of the Spanish Ministerio de Economía y Competitividad (MINECO) grant numbers: CGL2009-12703-C03-01 and CGL2009-12703-C03-02, the Consejería de Cultura y Turismo of the Junta de Castilla y León and the Fundación Atapuerca.

References

Adeloye, A., Kattan, K.R., Silverman, F.N., 1975. Thickness of the normal skull in the American Blacks and Whites. Am. J. Phys. Anthropol. 43, 23–30.

Alvernie, J.E., Fraser, K., Lanzino, G., 2006. The occipital artery: a microanatomical study. Neurosurgery 58, 114–122.

Anzelmo, M., Ventrice, F., Barbeito-Andrés, J., Pucciarelli, H.M., Sardi, M.L., 2014. Ontogenetic changes in cranial vault thickness in a modern sample of *Homo sapiens*. Am. J. Hum. Biol. 27, 475–485.

Arnold, L., Demuro, M., Parés, J.M., Pérez-González, A., Arsuaga, J.L., Bermúdez de Castro, J.M., Carbonell, E., 2014. Evaluating the suitability of extended-range luminescence dating techniques over Early and Middle Pleistocene timescales: published datasets and case studies from Atapuerca, Spain. Quat. Int. 289, 167–190, http://dx.doi.org/10.1016/j.quaint.2014.08.010.

Arnold, L.J., Demuro, M., 2015. Insights into TT-OSL signal stability from single-grain analyses of known-age deposits at Atapuerca, Spain. Quat. Geochronol. 30 (Part B), 472–478, http://dx.doi.org/10.1016/j.quageo.2015.02.005.

Arsuaga, J.L., Martínez, I., Lorenzo, C., Gracia, A., Muñoz, A., Alonso, O., Gallego, J., 1999. The human cranial remains from Gran Dolina Lower Pleistocene site (Sierra de Atapuerca, Spain). J. Hum. Evol. 37, 431–457.

Arsuaga, J.L., Martinez, I., Arnold, L.J., Aranburu, A., Gracia-Tellez, A., Sharp, W.D., Quam, R.M., Falgueres, C., Pantoja-Perez, A., Bischoff, J., Poza-Rey, E., Pares, J.M., Carretero, J.M., Demuro, M., Lorenzo, C., Sala, N., Martinon-Torres, M., Garcia, N., de Velasco, A., 2014. Neandertal roots: cranial and chronological evidence from Sima de los Huesos. Science 344, 1358–1363.

Baab, K.L., Freidline, S.E., Wang, S.L., Hanson, T., 2010. Relationship of cranial robusticity to cranial form, geography and climate in *Homo sapiens*. Am. J. Phys. Anthropol. 141, 97–115.

Balzeau, A., 2013. Thickened cranial vault and parasagittal keeling: correlated traits and autapomorphies of *Homo erectus*? J. Hum. Evol. 64, 631–644.

Balzeau, A., Grimaud-Hervé, D., Jacob, T., 2005. Internal cranial features of the Mojokerto child fossil (East Java, Indonesia). J. Hum. Evol. 48, 535–553.

Bennike, P., 2008. Trauma. In: Pinhasi, R., Mays, S. (Eds.), Advances in Human Palaeopathology. John Wiley & Sons Ltd., Chichester, pp. 309–328.

Berger, G.W., Pérez-González, A., Carbonell, E., Arsuaga, J.L., Bermúdez de Castro, J.M., Ku, T.L., 2008. Luminescence chronology of cave sediments at the Atapuerca paleoanthropological site, Spain. J. Hum. Evol. 55, 300–311.

Bermúdez de Castro, J.M., Arsuaga, J.L., Carbonell, E., Rosas, A., Martínez, I., Mosquera, M., 1997. A hominid from the Lower Pleistocene of Atapuerca, Spain: possible ancestor to Neandertals and modern humans. Science 276, 1392–1395.

Bermúdez de Castro, J.M., Carbonell, E., Cáceres, I., Díez, J.C., Fernández-Jalvo, Y., Mosquera, M., Ollé, A., Rodríguez, J., Rodríguez, X.P., Rosas, A., Rosell, J., Sala, R., Vergès, J.M., van der Made, J., 1999. The TD6 (Aurora Stratum) hominid site. Final remarks and new questions. J. Hum. Evol. 37, 695–700.

Bermúdez de Castro, J.M., Pérez-González, A., Martinón-Torres, M., Gómez-Robles, A., Rosell, J., Prado, L., Sarmiento, S., Carbonell, E., 2008. A new Early Pleistocene hominin mandible from Atapuerca-TD6, Spain. J. Hum. Evol. 55, 729–735.

Bermúdez de Castro, J.M., Martín-Francés, L., Modesto-Mata, M., Martínón-Torres, M., Martínez de Pinillos, M., García-Campos, C., Carretero, J.M., 2015a. Brief communication: virtual reconstruction of the Early Pleistocene mandible ATD6-96 from Gran Dolina-TD6-2 (Sierra de Atapuerca, Spain). Am. J. Phys. Anthropol. 159, 729–736, http://dx.doi.org/10.1002/ajpa.22919.

Bermúdez de Castro, J.M., Martinón-Torres, M., Martín-Francés, L., Modesto, M., Martínez de Pinillos, M., García, C., Carbonell, E., 2015b. *Homo antecessor*. The state of the art eighteen years later. Quatern. Int., http://dx.doi.org/10.1016/j.quaint.2015.03.049.

Boryslawski, K., Kurlej, W., Gworys, B., 2002. Changeability of emissary vein foramina based on modern skull material. Dent. Med. Probl. 39, 177–182.

Boyd, G.I., 1930. The emissary foramina of the cranium in man and the anthropoids. J. Anat. 65, 108–121.

Boylston, A., 2000. Evidence for weapon-related trauma in British archaeological samples. In: Cox, M., Mays, S. (Eds.), Human Osteology in Archaeology and Forensic Science. Greenwich Medical Media, London, pp. 357–380.

Braga, J., Boesch, C., 1997. Further data about venous channels in South African Plio-Pleistocene hominids. J. Hum. Evol. 33, 423–447.

Brain, C.K., 1993. A taphonomic overview of the Swartkrans fossil assemblages. In: Brain, C.K. (Ed.), Swartkrans, a Cave's Chronicle of Early Man. Transvaal Museum Monograph, Pretoria, pp. 257–264.

Brown, T., Pinkerton, S.K., Lambert, W., 1979. Thickness of the cranial vaultin Australian aboriginals. Arch. Phys. Anthropol. Oceania 14, 54–71.

Bruner, E., 2004. Geometric morphometrics and paleoneurology: brain shape evolution in genus *Homo*. J. Hum. Evol. 47, 279–303.

Bruner, E., 2015. Functional craniology and brain evolution. In: Bruner, E. (Ed.), Human Paleoneurology. Springer, Cham, pp. 57–94.

Bruner, E., Sherkat, S., 2008. The middle meningeal artery: from clinics to fossils. Child's Nerv. Syst. 24, 1289–1298.

Bruner, E., Pearson, O., 2013. Neurocranial evolution in modern humans: the case of Jebel Irhoud 1. Anthropol. Sci. 121, 31–41.

Bruner, E., Manzi, G., Arsuaga, J.L., 2003. Encephalization and allometric trajectories in the genus *Homo*: evidence from the Neanderthal and modern lineages. Proc. Natl. Acad. Sci. U S A 100, 15335–15340.

Bruner, E., Mantini, S., Perna, A., Maffei, C., Manzi, G., 2005. Fractal dimension of the middle meningeal vessels: variation and evolution in *Homo erectus*, Neanderthals, and modern humans. Eur. J. Morphol. 42, 217–224.

Bruner, E., Mantini, S., Ripani, M., 2009. Landmark-based analysis of the morphological relationship between endocranial shape and traces of the middle meningeal vessels. Anat. Rec. 292, 518–527.

Bruner, E., de la Cuétara, J.M., Holloway, R., 2011a. A bivariate approach to the variation of the parietal curvature in the Genus *Homo*. Anat. Rec. 294, 1548–1556.

Bruner, E., Mantini, S., Musso, F., de la Cuétara, J.M., Ripani, M., Sherkat, S., 2011b. The evolution of the meningeal vascular system in the human genus: from brain shape to thermoregulation. Am. J. Hum. Biol. 23, 35–43.

Bruner, E., Grimaud-Hervé, D., Wu, X., De la Cuétara, J.M., Holloway, R.L., 2015. A paleoneurological survey of *Homo erectus* endocranial metrics. Quatern. Int. 368, 80–87.

Buikstra, J.E., Uberlaker, D.H., 1994. Standards for Data Collection from Human Skeletal Remains. Arkansas Archaeological Survey Research Series 44. Archaeological Survey, Fayetteville.

Campaña, I., Benito-Calvo, A., Pérez-González, A., Ortega, A.I., Bermúdez de Castro, J.M., Carbonell, E., 2015. Pleistocene sedimentary facies of the Gran Dolina archaeo-paleoanthropological site (Sierra de Atapuerca, Burgos, Spain). Quatern. Int., http://dx.doi.org/10.1016/j.quaint.2015.04.023.

Carbonell, E., Bermúdez de Castro, J.M., Arsuaga, J.L., Díez, J.C., Rosas, A., Cuenca-Bescós, G., Sala, R., Mosquera, M., Rodriguez, X.P., 1995. Lower Pleistocene hominids and artifacts from Atapuerca-TD6 (Spain). Science 269, 826–830.

Carbonell, E., García-Antón, M.D., Mallol, C., Mosquera, M., Ollé, A., Rodríguez, X.P., Sahnouni, M., Sala, R., Vergès, J.M., 1999. The TD6 level lithic industry from Gran Dolina (Burgos, Spain): production and use. J. Hum. Evol. 37, 653–693.

Carbonell, E., Bermúdez de Castro, J.M., Arsuaga, J.L., Allue, E., Bastir, M., Benito, A., Cáceres, I., Canals, T., Díez, J.C., van der Made, J., Mosquera, M., Ollé, A., Pérez-González, A., Rodríguez, J., Rodríguez, X.P., Rosas, A., Rosell, J., Sala, R., Vallverdú, J., Vergés, J.M., 2005. An Early Pleistocene hominin mandible from Atapuerca-TD6, Spain. Proc. Natl. Acad. Sci. U S A 102, 5674–5678.

Carbonell, E., Cáceres, I., Lozano, M., Saladié, P., Rosell, J., Lorenzo, C., Vallverdú, J., Huguet, R., Canals, T., Bermúdez de Castro, J.M., 2010. Cultural cannibalism as a paleoeconomic system in the European Lower Pleistocene. Curr. Anthropol. 51, 539–549.

Copes, L.E., Kimbel, W.H., 2016. Cranial vault thickness in primates: *Homo erectus* does not have uniquely thick vault bones. J. Hum. Evol. 90, 120–134.

Cuenca-Bescós, G., Laplana, C., Canudo, J.I., 1999. Biochronological implications of the Arvicolidae (Rodentia, Mammalia) from the Lower Pleistocene hominid-bearing level of Trinchera Dolina 6 (TD6, Atapuerca, Spain). J. Hum. Evol. 37, 353–373.

Cuenca-Bescós, G., Blain, H.A., Rofes, J., Lozano-Fernández, I., López-García, J.M., Duval, M., Galán, J., Núñez-Lahuerta, C., 2015. Comparing two different Early Pleistocene microfaunal sequences from the caves of Atapuerca, Sima del Elefante and Gran Dolina (Spain): Biochronological implications and significance of the Jaramillo subchron. Quatern. Int. 389, 148–158, http://dx.doi.org/10.1016/j.quaint.2014.12.059.

Curnoe, D., 2009. Possible causes and significances of cranial robusticity among Pleistocene–Early Holocene Australians. J. Archaeol. Sci. 36, 980–990.

Eisová, S., Rangel de Lázaro, G., Píšová, H., Pereira-Pedro, S., Bruner, E., 2016. Parietal bone thickness and vascular diameters in adult modern humans: a survey on cranial remains. Anat. Rec. (accepted manuscript).

Falguères, C., Bahain, J.J., Yokoyama, Y., Arsuaga, J.L., Bermúdez de Castro, J.M., Carbonell, E., Bischoff, J.L., Dolo, J.M., 1999. Earliest humans in Europe: the age of Atapuerca fossils, Spain. J. Hum. Evol. 37, 343–352.

Falk, D., 1993. Meningeal arterial patterns in great apes: implications for hominid vascular evolution. Am. J. Phys. Anthropol. 92, 81–97.

Falk, D., Nicholls, P., 1992. Meningeal arteries in rhesus macaques (*Macaca mulatta*): implications for vascular evolution in anthropoids. Am. J. Phys. Anthropol. 89, 299–308.

Fernández-Jalvo, Y., Díez, J.C., Cáceres, I., Rosell, J., 1999. Human cannibalism in the Early Pleistocene of Europe (Gran Dolina, Sierra de Atapuerca, Burgos, Spain). J. Hum. Evol. 37, 591–622.

García, N., Arsuaga, J.L., 1999. Carnivores from the Early Pleistocene hominid-bearing Trinchera Dolina 6 (Sierra de Atapuerca, Spain). J. Hum. Evol. 37, 415–430.

García Gil, O.G., Cambra-Moo, O., Gil, J.A., Nacarino-Meneses, C., Barbero, M.A.R., Pérez, J.R., Martín, A.G., 2015. Investigation hisomorpholgical

variations in human cranial bones through ontogeny. C. R. Palevol., http://dx.doi.org/10.1016/j.crpv.2015.04.006.
Gauld, S.C., 1996. Allometric patterns of cranial bone thickness in fossil hominins. Am. J. Phys. Anthropol. 100, 411–426.
Gil, E., Aguirre, E., Hoyos, M., 1987. Contexto estratigráfico. In: Aguirre, E., Carbonell, E., Bermúdez de Castro, J.M. (Eds.), El Hombre Fósil de Ibeas y el Pleistoceno de la Sierra de Atapuerca. Monografías de la Junta de Castilla y León, Valladolid, pp. 47–54.
Grimaud-Hervé, D., 1997. L'évolution de l'encéphale chez *Homo erectus* et *Homo sapiens*. Exemples de l'Asie et de l'Europe. Cahiers de Paléoanthropologie. CNRS Éditions, Paris.
Grossman, C.B., Potts, D.G., 1974. Arachnoid granulations: radiology and anatomy. Radiology 113, 95–100.
Gunz, P., Neubauer, S., Maureille, B., Hublin, J.J., 2010. Brain development after birth differs between Neanderthals and modern humans. Curr. Biol. 20, R921–R922.
Hammer, O., Harper, D.A.T., Ryan, P.D., 2001. PAST: paleontological statistics software package for education and data analysis. Palaentol. Electr. 4, 1–9.
Hatipoglu, H.G., Ozcan, H.N., Hatipoglu, U.S., Yuksel, E., 2008. Age, sex and body mass index in relation to calvarial diploe thickness and craniometric data on MRI. Forensic Sci. Int. 182, 46–51.
Hershkovitz, I., Greenwald, C., Rothschild, B.M., Latimer, B., Dutour, O., Jellema, L.M., Wish-Baratz, S., Pap, I., Leonetti, G., 1999. The elusive diploic veins: anthropological and anatomical perspective. Am. J. Phys. Anthropol. 108, 345–358.
Holloway, R.L., 1981. Exploring the dorsal surface of hominoid brain endocasts by stereoplotter and discriminant analysis. Philos. Trans. R. Soc. London, Ser. B. 393, 155–166.
Hwang, K., Hollinger, J.O., Chung, R.S., Lee, S.I., 2000. Histomorphometry of parietal bones versus age and race. J. Craniofac. Surg. 11, 17–23.
Jung, Y.S., Kim, H.J., Chod, S.W., Kang, J.W., Cha, I.H., 2003. Regional thickness of parietal bone in Korean adults. Int. I. Oral. Maxillofac. Surg. 32, 638–641.
Kennedy, G.E., 1991. On the autapomorphic traits of *Homo erectus*. J. Hum. Evol. 20, 375–412.
Knott, J.F., 1881. On the cerebral sinuses and their variations. J. Anat. Physiol. 16, 27–42.
Lang, J., Brückner, B., 1981. Üner dicke und dümme Zonen des Neurocranium. Impressiones gyrorum und Foramina parietalia bei Kindem und Erwachsenen.
Le Gros Clark, W.E., 1920. On the Pacchionian bodies. J. Anat. 55, 40–48.
Li, Q., Pan, S.N., Yin, Y.M., Li, W., Chen, Z.A., Liu, Y.H., Wu, Z.H., Guo, Q.Y., 2011. Normal cranial bone marrow MR imaging pattern with age-related ADC value distribution. Eur. J. Radiol. 80, 471–477.
Lieberman, D.E., 1996. How and why humans grow thin skulls: experimental evidence for systemic cortical robusticity. Am. J. Phys. Anthropol. 101, 217–236.
Love, J., Derrick, S., Wiersema, J., 2011. Skull fractures. In: Love, J., Derrick, S., Wiersema, J. (Eds.), Skeletal Atlas of Child Abuse. Human Press, London, pp. 9–37.
Lynnerup, N., 2001. Cranial thickness in relation to age, sex and general body build in a Danish forensic sample. Forensic Sci. Int. 117, 45–51.
van der Made, J., 1999. Ungulates from Atapuerca-TD6. J. Hum. Evol. 37, 389–413.
Marsh, H.E., 2013. Beyond thick versus thin: mapping cranial vault thickness patterns in recent *Homo sapiens*. University of Iowa, IA, USA.
Menegaz, R.A., Sublett, S.V., Figueroa, S.D., Hoffman, T.J., Ravosa, M.J., Aldridge, K., 2010. Evidence for the influence of diet on cranial form and robusticity. Anat. Rec. 293, 630–641.
Minugh-Purvis, N., (PhD Dissertation) 1988. Patterns of Craniofacial Growth and Development in Upper Pleistocene Hominids. University of Pennsylvania, Michigan Microfilms, Ann Arbor.
Moreno, D., Falguères, C., Pérez-González, A., Voinchet, P., Ghaleb, B., Despriee, J., Bahain, J.-J., Sala, R., Carbonell, E., Bermúdez de Castro, J.M., Arsuaga, J.L., 2015. New radiometric dates on the lowest stratigraphical section (TD1 to TD6) of Gran Dolina site (Atapuerca, Spain). Quat. Geochronol. 30, 535–540, http://dx.doi.org/10.1016/j.quageo.2015.05.007.
Nawrocki, S.P., (PhD Dissertation) 1991. A Biomechanical Model of Cranial Vault Thickness in Archaic *Homo*. SUNY Binghamton, New York.
Neubauer, S., Gunz, P., Hublin, J.-J., 2009. The pattern of endocranial ontogenetic shape changes in humans. J. Anat. 215, 240–255.
Neubauer, S., Gunz, P., Hublin, J.-J., 2010. Endocranial shape changes during growth in chimpanzees and humans: a morphometric analysis of unique and shares aspects. J. Hum. Evol. 59, 555–566.
Ortner, D.J., 2003. Trauma. In: Ortner, D.J. (Ed.), Identification of Pathological Conditions in Human Skeletal Remains. Academic Press, San Diego, pp. 119–178.
Panteado, C.V., Santo Neto, H., 1985. The number and location of the parietal foramen in human skulls. Anat. Anz. 158, 39–41.
Parés, J.M., Pérez-González, A., 1995. Paleomagnetic age for hominid fossils at Atapuerca Archaeological site, Spain. Science 269, 830–832.
Parés, J.M., Pérez-González, A., 1999. Magnetochronology and stratigraphy at Gran Dolina section, Atapuerca (Burgos, Spain). J. Hum. Evol. 37, 325–342.
Peterson, J., Dechow, P.C., 2002. Material properties of the inner and outer cortical tables of the human parietal bone. Anat. Rec. 268, 7–15.
Rangel de Lázaro, G., de la Cuatara, J.M., Píšová, H., Lorenzo, C., Bruner, E., 2015. Diploic vessels and computed tomography: segmentation and comparison in modern humans and fossil hominids. Am. J. Phys. Anthropol. 159, 313–324.
Rightmire, G.P., 2008. *Homo* in the Middle Pleistocene: hypodigms, variation, and species recognition. Evol. Anthropol. 17, 8–21.
Roche, A.F., 1953. Increase in cranial thickness during growth. Hum. Biol. 25, 81–92.
Saban, R., 1995. Image of the human fossil brain: endocranial casts and meningeal vessels in young and adult subjects. In: Changeux, J.-P., Chavaillon, J. (Eds.), Origins of the Human Brain. Clarendon Press, Oxford, pp. 11–38.
Sala, N., Arsuaga, J.L., Pantoja-Pérez, A., Pablos, A., Martínez, I., Quam, R.M., Gómez-Olivencia, A., Bermúdez de Castro, J.M., Carbonell, E., 2015. Lethal interpersonal violence in the Middle Pleistocene. PLoS One 10, e0126589.
Saladié, P., Huguet, R., Rodríguez-Hidalgo, A., Cáceres, I., Esteban-Nadal, M., Arsuaga, J.L., Bermúdez de Castro, J.M., Carbonell, E., 2012. Intergroup cannibalism in the European Early Pleistocene: the range expansion and imbalance of power hypotheses. J. Hum. Evol. 63, 682–695.
Sauer, N., 1998. The timing of head injuries and manner of death: distinguishing among antemortem, peri-mortem and postmortem trauma. In: Reichs, N. (Ed.), Forensic Osteology. Charles C. Thomas, Springfield, pp. 321–332.
Schelling, F., 1978. Die Emissarien des menschlichen Schädels. Anat. Anz. 143, 340–382.
Schneider, C.A., Rasband, W.S., Eliceiri, K.W., 2012. NIH Image to ImajeJ: 25 years of image analysis. Nat. Methods 9, 671–675.
Scott, N., Neubauer, S., Hublin, J.-J., Gunz, P., 2014. A shared pattern of postnatal endocranial development in extant hominoids. Evol. Biol. 41, 572–594.
Stallworthy, J.A., 1932. A case of enlarged parietal foramina associated with metopism and irregular synostosis of the coronal suture. J. Anat. 67, 168–174.
Stringer, C.B., 2012. The status of *Homo heidelbergensis* (Schoetensack, 1908). Evol. Anthropol. 21, 101–107.
Torres-Lagares, D., Tulasne, J.-F., Pouqet, C., Llorens, A., Saffar, J.-L., Lesclous, P., 2010. Structure and remodeling of the human parietal bone: and age and gender histomorphometric study. J. Craniomaxillofac. Surg. 38, 325–330.
Tsutsumi, S., Nakamura, M., Tabuchi, T., Yasumoto, Y., Ito, M., 2013. Calvarial diploic venous channels: an anatomic study using high-resolution magnetic resonance imaging. Surg. Radiol. Anat. 35, 935–941.
Waldron, T., 2009. Trauma. In: Waldron, T. (Ed.), Paleopathology. Cambridge University Press, Cambridge, pp. 138–167.
Wu, X., Schepartz,J., Liu, L.A., Trinkaus, W.E., 2011. Antemortem trauma and survival in the late Middle Pleistocene human cranium from Maba, South China. Proc. Natl. Acad. Sci. U S A 108, 19558–19562.
Yoshioka, N., Rhoton, A.L., Abe, H., 2006. Scalp to meningeal arterial anastomosis in the parietal foramen. Neurosurgery 58, 123–126.
Zenker, W., Kubik, S., 1996. Brain cooling in humans – anatomical considerations. Anat. Embryol. 193, 1–13.